AGU PUBLICATIONS

JGR

Journal of Geophysical Research: Space Physics

RESEARCH ARTICLE
10.1002/2016JA022587

Key Points:
- Suprathermal populations in the solar wind
- The interplay of the core and suprathermal populations
- Kinetic instabilities: energy transfer between plasma populations

Correspondence to:
S. M. Shaaban,
shaaban.mohammed@student.kuleuven.be

Citation:
Shaaban, S. M., M. Lazar, S. Poedts, and A. Elhanbaly (2016), The interplay of the solar wind proton core and halo populations: EMIC instability, *J. Geophys. Res. Space Physics*, *121*, 6031–6047, doi:10.1002/2016JA022587.

Received 22 FEB 2016
Accepted 10 JUN 2016
Accepted article online 20 JUN 2016
Published online 9 JUL 2016

The interplay of the solar wind proton core and halo populations: EMIC instability

S. M. Shaaban[1,2], M. Lazar[3,4], S. Poedts[1], and A. Elhanbaly[2]

[1]Centre for Mathematical Plasma Astrophysics, Leuven, Belgium, [2]Theoretical Physics Research Group, Physics Department, Faculty of Science, Mansoura University, Mansoura, Egypt, [3]Institut für Theoretische Physik, Lehrstuhl IV: Weltraum- und Astrophysik, Ruhr-Universität Bochum, Bochum, Germany, [4]Royal Belgian Institute for Space Aeronomy 3-Avenue Circulaire, Brussels, Belgium

Abstract The kinetic properties of the solar wind protons (ions), like their temperature anisotropy and the resulting instabilities, are, in general, investigated considering only the proton core (or thermal) populations. The implication of the suprathermal halo components is minimized or just ignored, despite the fact that their presence in the solar wind is continuously reported by the observations, and their kinetic energy density may be significant. Whether they are originating in the corona or solar wind, the energetic particles may result from acceleration by the plasma turbulence or from the pitch angle scattering of the streaming protons by the self-generated fluctuations. The presence of suprathermal protons in the heliosphere suggests, therefore, a direct implication in resonant interactions, e.g., Landau and cyclotron, with plasma particles. This paper presents the results of a first investigation on the interplay of the proton core and suprathermal halo, when both these two populations may exhibit temperature anisotropies, which destabilize the electromagnetic ion (proton) cyclotron (EMIC) modes. These results clearly show that for conditions typically encountered in the solar wind, the effects of the suprathermals can be more important than those driven by the core. Remarkable are also the cumulative effects of the core and halo components, which change dramatically the instability conditions.

1. Introduction

The solar wind plasma particles are not in thermal equilibrium. Measured in situ, the velocity distributions of plasma particles, mainly, electrons and protons, show, in general, important deviations from a Maxwellian shape, especially determined by the presence of suprathermal populations [*Lin*, 1998; *Lazar et al.*, 2012]. Forming the so-called halo components, these populations enhance the high-energy tails of the velocity distributions which are well described by the power law or Kappa distribution functions [*Vasyliunas*, 1968; *Christon et al.*, 1989; *Collier et al.*, 1996; *Pierrard and Lazar*, 2010].

On the other hand, the solar wind is a hot and dilute plasma, where particle-particle collisions are not efficient to establish the equilibrium. The ubiquitious presence of suprathermal particles confirms this hypothesis and also suggests the existence of a mechanism of acceleration and energization of plasma particles. There are different physical mechanisms invoked in the particle acceleration, and one of the most efficient interactions occurs by Landau or cyclotron resonances with plasma waves and fluctuations at kinetic electron and ion (proton) scales. These fluctuations are permanently reported by the observations [*Jian et al.*, 2009; *Bruno and Carbone*, 2013] and may have the origin either in the large-scale perturbations produced by the coronal plasma injections and then transported and decayed in the super-Alfvénic solar wind or may be enhanced locally by the kinetic instabilities driven by the anisotropy of plasma particles, e.g., the biaxis temperature anisotropy of the gyrotropic distributions observed in the solar wind and terrestrial magnetosphere (see the review by *Marsch* [2006] and references therein). In the absence of collisions it is indubitable that the plasma waves and fluctuations must play a major role triggering the transport of particles and energy in these environments.

A rigorous prediction/description of the wave fluctuations can be achieved by a kinetic treatment of the unstable plasma states and the resulting instabilities using realistic models for the velocity distribution functions (VDFs) of plasma particles. Widely used are the Maxwellian (standard) models [*Gary*, 1993; *Shaaban et al.*, 2015], which describe well the main (thermal) core of the distribution with different anisotropies,

e.g., bi-Maxwellian to describe a (biaxis) temperature anisotropy, or a drifting-Maxwellian to incorporate streaming components. Standard models were also invoked to describe the suprathermal halo populations [*Feldman et al.*, 1975; *Gary et al.*, 1996; *Maksimovic et al.*, 2000], despite the fact that the enhanced suprathermal tails of the distribution are not well represented without the Kappa power law.

There is indeed a strong evidence that the entire distribution function can be well adjusted by a superposition of a Maxwellian core and one or more power law distributions [*Feldman et al.*, 1973; *Marsch et al.*, 1982; *Christon et al.*, 1991; *Sittler and Burlaga*, 1998; *Maksimovic et al.*, 2005; *Nieves-Chinchilla and Viñas*, 2008]. (A field-aligned strahl may eventually be present as a secondary suprathermal component more pronounced in the energetic events like fast winds or coronal mass ejections). In theoretical predictions the anisotropic Kappa, e.g., bi-Kappa and product-bi-Kappa, are introduced as global models (see the reviews by *Hellberg et al.* [2005] and *Pierrard and Lazar* [2010]), incorporating both the core and halo populations in the same global Kappa which is nearly Maxwellian at low energies and decreasing as power law at high energies. The advantage is that a single (global) Kappa simplifies the approach and implicitly the computations, especially for the anisotropic models with an increased number of parameters. However, a global Kappa couples unrealistically the core and halo populations describing them with the same parameters, i.e., the same density, temperature, and temperature anisotropy, and, therefore, poorly representing the true distribution and leading to questionable results [*Lazar*, 2012].

The number of parameters increases considerably if one considers the core and halo as two distinct and anisotropic components, i.e., an anisotropic bi-Maxwellian core (subscript c) with density n_c, two components of the temperature $T_{c,\parallel}$ and $T_{c,\perp}$, see equations (2)–(4) below, an anisotropic bi-Kappa halo (subscript h) with n_h, two components of the temperature $T_{h,\parallel}$ and $T_{h,\perp}$, and the power index κ to quantify the presence of suprathermal populations, see equations (5)–(8) below. In a recent endeavor to provide a realistic description for the electromagnetic electron cyclotron (EMEC) instability in the solar wind conditions, *Lazar et al.* [2014, 2015a] have shown that such a complex but realistic model is computationally tractable and yields results markedly different than simplified models used before.

Besides the EMEC (or whistler) instability, the electromagnetic ion cyclotron (EMIC) instability plays an equally important role in the solar wind and the subsequent plasma structures, like planetary magnetospheres. Driven by plasma particles with an excess of transverse temperature $T_\perp > T_\parallel$, these instabilities enhance the electromagnetic fluctuations near the cyclotron frequency. The same mechanism of cyclotron resonance may also ensure the transfer of energy in opposite direction by dissipating the electromagnetic fluctuations and heating plasma particles. From the entire spectrum of electromagnetic fluctuations decaying in the solar wind [*Mangeney et al.*, 2001; *Bruno and Carbone*, 2013], the EMIC waves near the ion (or proton) cyclotron frequency Ω_p are the first dissipative fluctuations linking two distinct regimes, namely, that of the large-scale (fluid) fluctuations of frequency much below Ω_p and the kinetic regime of high-frequency waves with phase velocity close to the thermal velocity of plasma particles.

The EMIC instability has been extensively investigated, but the existing studies of the solar wind plasma conditions are limited to simplified models of the VDFs of plasma particles, which facilitate the computations and characterization of the unstable solutions. Thus, early studies have ignored the suprathermal populations, assuming bi-Maxwellian distributed plasmas and providing basic properties of the cyclotron instabilities (see the textbook by *Gary* [1993] and references therein). The effects of suprathermal protons on the EMIC instability are mainly interpreted using a global bi-Kappa model for the anisotropic protons, see the reviews by *Hellberg et al.* [2005] and *Pierrard and Lazar* [2010], and the progress made by *Astfalk et al.* [2015]; *dos Santos et al.* [2015] in numerical techniques to resolve the stability of anisotropic Kappa distributed plasmas. Moreover, recent studies have shown that these effects are highly dependent on the shape of the distribution by contrasting to a product bi-Kappa which introduces an excess of free energy and stimulates the instability [*Lazar*, 2012; *Lazar and Poedts*, 2014; *dos Santos et al.*, 2015]. More advanced models, which assume two distinct components, namely, a core and a halo, were also considered, but with limitations, either minimizing the effects of suprathermals by considering both the core and halo populations bi-Maxwellian distributed [*Gary et al.*, 1996] or neglecting completely thermal effects of the core by considering this component cold, i.e., $T_c \to 0$ [*Xiao et al.*, 2007].

Nonlinear regimes of the EMIC instability are usually investigated in numerical (hybrid) simulations, revealing the potential implication of this instability in many key processes in space plasmas. Thus, the role played by this instability in mediating the energetic transfer between different species and populations of plasma particles

may explain the contribution of the core anisotropy to the formation of additional beaming components, acceleration of alpha particles and non-Maxwellian distribution functions [*Araneda et al.*, 2008; *Hellinger and Trávníček*, 2011; *Ofman et al.*, 2014; *Maneva et al.*, 2015]. The nonlinear EMIC waves can lead to preferentially heat and accelerate the solar wind plasma [*Ofman et al.*, 2002], affecting the wave-particle interactions and the shape of the ion VDF [*Maneva et al.*, 2015]. Moreover, the ion acceleration and anisotropic heating caused by these nonlinear waves lead to deviations from thermal Maxwellian equilibrium and eventually the formation of the ion beams along the direction of the ambient magnetic field [*Araneda et al.*, 2008].

In this paper we propose a new linear approach of the EMIC instability on the basis of a realistic kinetic model of the proton VDF, which combines a bi-Maxwellian core and a bi-Kappa halo populations. A linear dispersion and stability analysis is of interest for a basic characterization of the instability conditions, providing important information about the instability nature, e.g., periodic or aperiodic, and nevertheless about the instability thresholds and the most unstable (fastest growing) modes which are usually invoked by the nonlinear approaches. The new approach proposed here enables us to study for the first time the interplay of the thermal core and suprathermal halo, especially when both these two components are anisotropic. Our study is focused on the solar wind conditions which destabilize the EMIC modes. To keep the analysis straightforward, at this stage we neglect the influence of alpha particles and isolate only the effects obtained from the interplay of proton core and halo populations using the linear Vlasov theory. Although a minor constituent of the solar wind plasma, alpha particles may change both the linear and nonlinear dispersive properties [*Cornwall and Schulz*, 1971; *Hellinger and Trávníček*, 2005; *Matteini et al.*, 2007; *Maruca et al.*, 2012]. Thus, investigations by *Maruca et al.* [2012] have not taken into account the suprathermal populations and any relative flow between different species of plasma particles and concluded that the effect of alpha particles on the anisotropy threshold of the proton cyclotron instability is relatively small because protons dominate in the number density. However, in the fast winds the presence of an alpha/proton velocity drift as a source of free energy for beam-type instabilities cannot be neglected and must be included in the calculation of the stability thresholds [*Hellinger and Trávníček*, 2005; *Matteini et al.*, 2007].

The present paper is organized as follows: In section 2 we introduce the velocity distribution models for the proton populations. The electrons are assumed isotropic, allowing us to isolate the effects of protons and quantify the individual contributions of the proton core and halo components. In section 3 we derive the dispersion relation for the EMIC modes and analyze the threshold conditions and unstable solutions by contrast to those provided before with simplified models. The results of the present study are summarized and discussed in section 4.

2. Dual Core-Halo Distributions

In the absence of strahl or beaming components, there is no relative drift between suprathermal and core populations. The velocity distribution functions measured in situ are gyrotropic and present a dual structure, namely, with a core (subscript c) and a halo (subscript h), for any sort of plasma particle (subscript $\alpha = e, p$ for electrons and protons, respectively)

$$F_\alpha\left(v_\parallel, v_\perp\right) = F_{\alpha,c}\left(v_\parallel, v_\perp\right) + F_{\alpha,h}\left(v_\parallel, v_\perp\right). \tag{1}$$

Each of these two components can exhibit a temperature anisotropy $A = T_\perp/T_\parallel \neq 1$ with respect to the uniform magnetic field. The core population is described by the unperturbed bi-Maxwellian distribution

$$F_{\alpha,c}\left(v_\parallel, v_\perp\right) = \frac{1}{\pi^{3/2} u_{\alpha,\perp}^2 u_{\alpha,\parallel}} \exp\left(-\frac{v_\parallel^2}{u_{\alpha,\parallel}^2} - \frac{v_\perp^2}{u_{\alpha,\perp}^2}\right), \tag{2}$$

with thermal velocities $u_{\alpha,\parallel,\perp}$ defined by

$$T_{c,\parallel}^M = \frac{m_\alpha}{k_B}\int \mathrm{d}\mathbf{v} v_\parallel^2 F_\alpha(v_\parallel, v_\perp) = \frac{m_\alpha u_{\alpha,\parallel}^2}{2k_B} \tag{3}$$

$$T_{c,\perp}^M = \frac{m_\alpha}{2k_B}\int \mathrm{d}\mathbf{v} v_\perp^2 F_\alpha(v_\parallel, v_\perp) = \frac{m_\alpha u_{\alpha,\perp}^2}{2k_B}. \tag{4}$$

The suprathermal (halo) tails are described by a bi-Kappa VDF [*Summers and Thorne*, 1991]

$$F_{\alpha,h} = \frac{1}{\pi^{3/2}\theta_{\alpha,\perp}^2\theta_{\alpha,\parallel}}\frac{\Gamma(\kappa+1)}{\Gamma(\kappa-1/2)}\left[1+\frac{v_\parallel^2}{\kappa\theta_{\alpha,\parallel}^2}+\frac{v_\perp^2}{\kappa\theta_{\alpha,\perp}^2}\right]^{-\kappa-1}. \tag{5}$$

This distribution function is normalized to unity $\int d^3v F_\alpha = 1$ and is written in terms of the generalized thermal velocities $\theta_{\alpha,\parallel,\perp}$, which are defined, for a power index $\kappa > 3/2$, by

$$T_{h,\parallel}^K = \frac{2\kappa}{2\kappa-3}\frac{m_\alpha\theta_{\alpha,\parallel}^2}{2k_B},\quad T_{h,\perp}^K = \frac{2\kappa}{2\kappa-3}\frac{m_\alpha\theta_{\alpha,\perp}^2}{2k_B}. \tag{6}$$

The halo temperature is increased with increasing the suprathermal populations [*Lazar et al.*, 2015b; *Shaaban et al.*, 2016], which are quantified by a finite power index κ,

$$T_{h,\parallel,\perp}^K = \frac{2\kappa}{2\kappa-3}T_{h,\parallel,\perp}^M > T_{h,\parallel,\perp}^M. \tag{7}$$

Implicitly, the plasma beta parameter $\beta = 8\pi n k_B T/B_0^2$ can be defined for each of the core and halo populations, and their parallel components used in our calculations read

$$\beta_{c,\parallel}^M = \frac{8\pi n_c k_B T_{c,\parallel}^M}{B_0^2},\quad \beta_{h,\parallel}^K = \frac{8\pi n_h k_B T_{h,\parallel}^K}{B_0^2} = \frac{2\kappa}{2\kappa-3}\beta_{h,\parallel}^M > \beta_{h,\parallel}^M, \tag{8}$$

Such a dual structure has been reported for both major species of space plasma particles, e.g., by *Feldman et al.* [1973], *Marsch et al.* [1982], and *Christon et al.* [1991] for protons and by *Vasyliunas* [1968], *Feldman et al.* [1975], *Maksimovic et al.* [1997], *Pierrard et al.* [1999], and *Maksimovic et al.* [2005] for electrons. In the present approach the electrons will be taken isotropic and sufficiently cold since our intention is to isolate and describe only the effects of the anisotropic protons on the instability of the EMIC modes.

3. Stability Analysis: EMIC Modes

We restrain to parallel modes since in the direction parallel to the stationary magnetic field $\boldsymbol{B_0}$, the EMIC instability is decoupled from the electrostatic modes and exhibits maximum growth rates [*Kennel and Petschek*, 1966]. For a collisionless and homogenous plasma of electrons and protons described by the core and halo distributions (2)–(8), the dispersion relations for the parallel electromagnetic modes read

$$\begin{aligned}\frac{c^2k^2}{\omega^2} = 1 &+ \sum_{\alpha=e,p}\frac{\omega_{\alpha,c}^2}{\omega^2}\left[\frac{\omega}{ku_{\alpha,\parallel}}Z\left(\xi_\alpha^\pm\right)+\left(A_{\alpha,c}-1\right)\left\{1+\xi_\alpha^\pm Z\left(\xi_\alpha^\pm\right)\right\}\right]\\ &+ \sum_{\alpha=e,p}\frac{\omega_{\alpha,h}^2}{\omega^2}\left[\frac{\omega}{k\theta_{\alpha,\parallel}}Z_\kappa\left(g_\alpha^\pm\right)+\left(A_{\alpha,h}-1\right)\left\{1+g_\alpha^\pm Z_\kappa\left(g_\alpha^\pm\right)\right\}\right],\end{aligned} \tag{9}$$

where ω is the wave frequency, k is the wave number, c is the light speed, $\omega_{\alpha,c,h}^2 = 4\pi n_{c,h}e^2/m_\alpha$ are the plasma frequencies of the core (subscript c) and halo (subscript h), $A_{\alpha,c,h} = \left(T_{\alpha,\perp}/T_{\alpha,\parallel}\right)_{c,h}$ are the temperature anisotropies, and $\pm$ denotes the circular polarizations, right handed (RH) and left handed (LH), respectively,. The dispersion relations are derived in terms of the plasma dispersion function [*Fried and Conte*, 1961]

$$Z\left(\xi_\alpha^\pm\right) = \frac{1}{\pi^{1/2}}\int_{-\infty}^{\infty}\frac{\exp\left(-x^2\right)}{x-\xi_\alpha^\pm}dt,\quad \Im\left(\xi_\alpha^\pm\right) > 0, \tag{10}$$

of argument

$$\xi_\alpha^\pm = \frac{\omega\pm\Omega_\alpha}{ku_{\alpha,\parallel}}, \tag{11}$$

and the modified (Kappa) dispersion function [*Lazar et al.*, 2008]

$$Z_\kappa\left(g_\alpha^\pm\right) = \frac{1}{\pi^{1/2}\kappa^{1/2}}\frac{\Gamma(\kappa)}{\Gamma(\kappa-1/2)}\int_{-\infty}^{\infty}\frac{\left(1+x^2/\kappa\right)^{-\kappa}}{x-g_\alpha^\pm}dx,\quad \Im\left(g_\alpha^\pm\right) > 0, \tag{12}$$

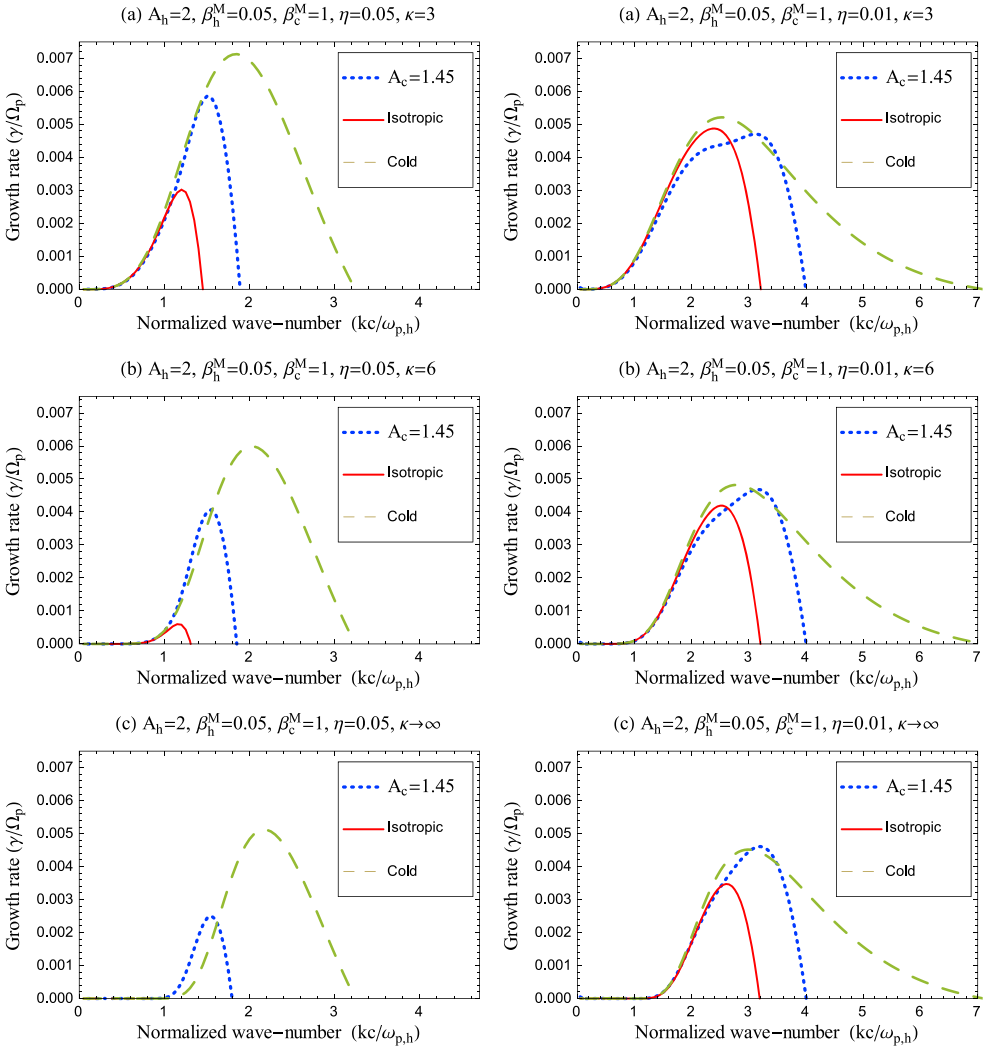

Figure 1. Comparison between the growth rates of the EMIC instability obtained with three distinct models for the core: cold (dashed lines), isotropic (solid lines), and anisotropic with $A_c = 1.45$ (dotted lines), two density ratios (left column) $\eta = 0.05$ and (right) $\eta = 0.01$, and different power indices (top tow) $\kappa = 3$, $\kappa = 6$ (middle), and (bottom) ∞. The other parameters are $A_h = 2$, $\beta_h^M = 0.05$, and $\beta_c^M = 1$.

of argument

$$g_\alpha^{\pm} = \frac{\omega \pm \Omega_\alpha}{k\theta_{\alpha,\|}}. \tag{13}$$

where $\Omega_\alpha = q_\alpha \boldsymbol{B}_0/m_\alpha c$ is the gyrofrequency (nonrelativistic).

If we neglect thermal effects of electrons, keeping only the zero-order term in the large argument ($|\xi_e|^+ \gg 1$) approximation of their dispersion function, the dispersion relation (9) for the EMIC modes (subluminal, $\omega^2 \ll k^2c^2$) with $\omega < \Omega_p \ll |\Omega_e|$ can be rewritten with normalized quantities as follows

$$\tilde{k}^2 = A_h - 1 + \frac{A_h(\tilde{\omega}-1)+1}{\tilde{k}\sqrt{\beta_{h,\|}^M}} Z_\kappa\left(\frac{\tilde{\omega}-1}{\tilde{k}\sqrt{\beta_{h,\|}^M}}\right) - \tilde{\omega} + \frac{1}{\eta}\left[A_c - 1 + \frac{A_c(\tilde{\omega}-1)+1}{\tilde{k}\sqrt{\eta\beta_{c,\|}^M}} \times Z\left(\frac{\tilde{\omega}-1}{\tilde{k}\sqrt{\eta\beta_{c,\|}^M}}\right) - \tilde{\omega}\right], \tag{14}$$

where $\tilde{\omega} = \omega/\Omega_p$, $\tilde{k} = kc/\omega_{p,h}$, $\beta_{c,\|}^M = 8\pi n_c k_B T_{c,\|}^M/B_0^2$, and $\beta_{h,\|}^M = 8\pi n_h k_B T_{h,\|}^M/B_0^2$ are the parallel proton beta parameter for the core and halo, respectively, and $\eta = n_h/n_c$ is the halo-core relative density.

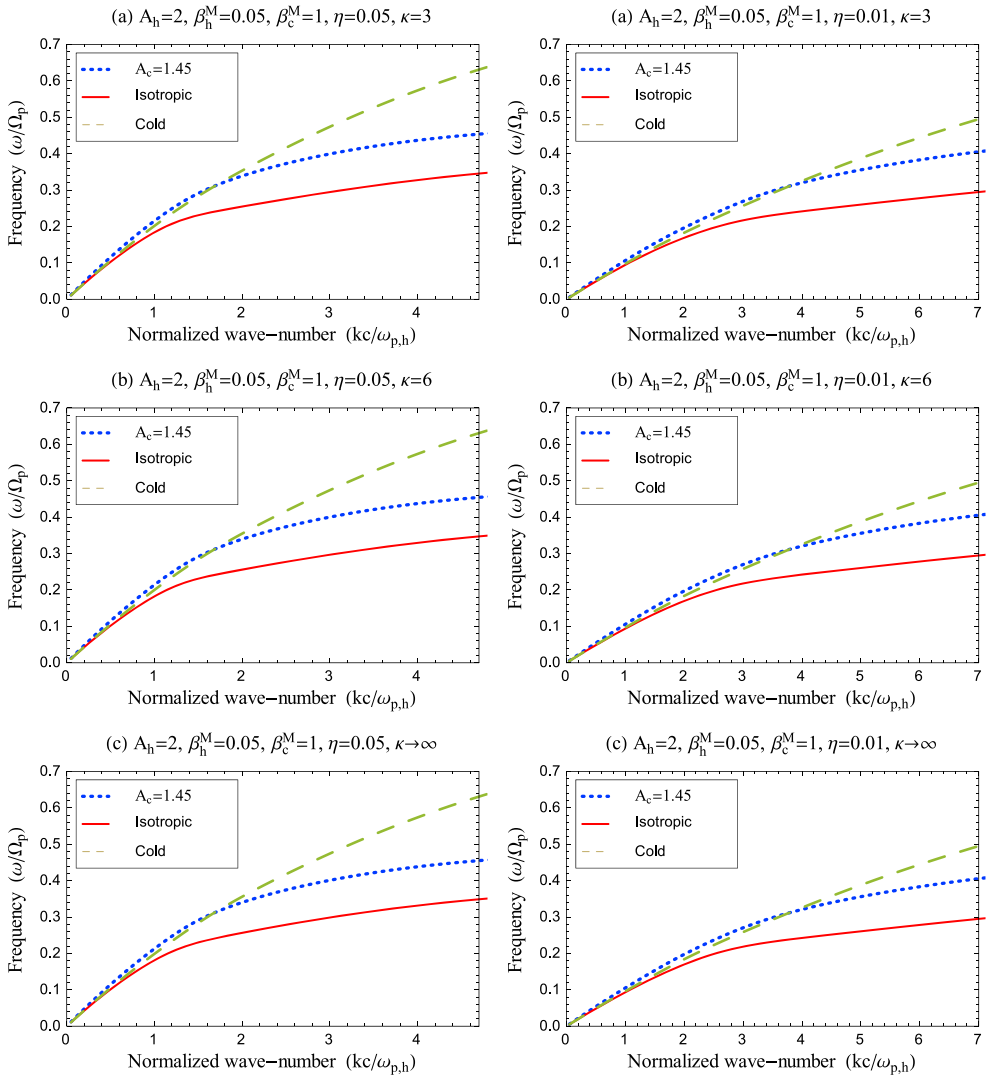

Figure 2. The wave frequency of the unstable EMIC modes in Figure 1.

The core may be less anisotropic than the halo, and if we take the core isotropic $A_c = 1$, the dispersion relation (14) reduces to

$$\tilde{k}^2 = A_h - 1 + \frac{A_h(\tilde{\omega}-1)+1}{\tilde{k}\sqrt{\beta_{h,\|}^M}} Z_\kappa\left(\frac{\tilde{\omega}-1}{\tilde{k}\sqrt{\beta_{h,\|}^M}}\right) + \frac{\tilde{\omega}}{\eta^{1.5}\tilde{k}\sqrt{\beta_{c,\|}^M}} Z\left(\frac{\tilde{\omega}-1}{\tilde{k}\sqrt{\eta\beta_{c,\|}^M}}\right) - \tilde{\omega} - \frac{\tilde{\omega}}{\eta}. \tag{15}$$

Moreover, if the core is cold enough, i.e., $T_c \to 0$, a situation however unrealistic for the solar wind, we may consider the zero-order approximation of the plasma dispersion function in the limit of very large arguments $Z(|\xi| \gg 1) = -\xi^{-1}$ and recover the dispersion relation derived by *Xiao et al.* [2007]

$$\tilde{k}^2 = A_h - 1 + \frac{A_h(\tilde{\omega}-1)+1}{\tilde{k}\sqrt{\beta_{h,\|}^M}} Z_\kappa\left(\frac{\tilde{\omega}-1}{\tilde{k}\sqrt{\beta_{h,\|}^M}}\right) - \frac{\tilde{\omega}}{\eta(\tilde{\omega}-1)} - \frac{\tilde{\omega}(\eta+1)}{\eta}. \tag{16}$$

3.1. The Unstable Solutions

In this section, we discuss the EMIC unstable solutions and identify the most relevant cases determined by the interplay of the core and halo populations and their influence on the growth rates, wave frequency, and the

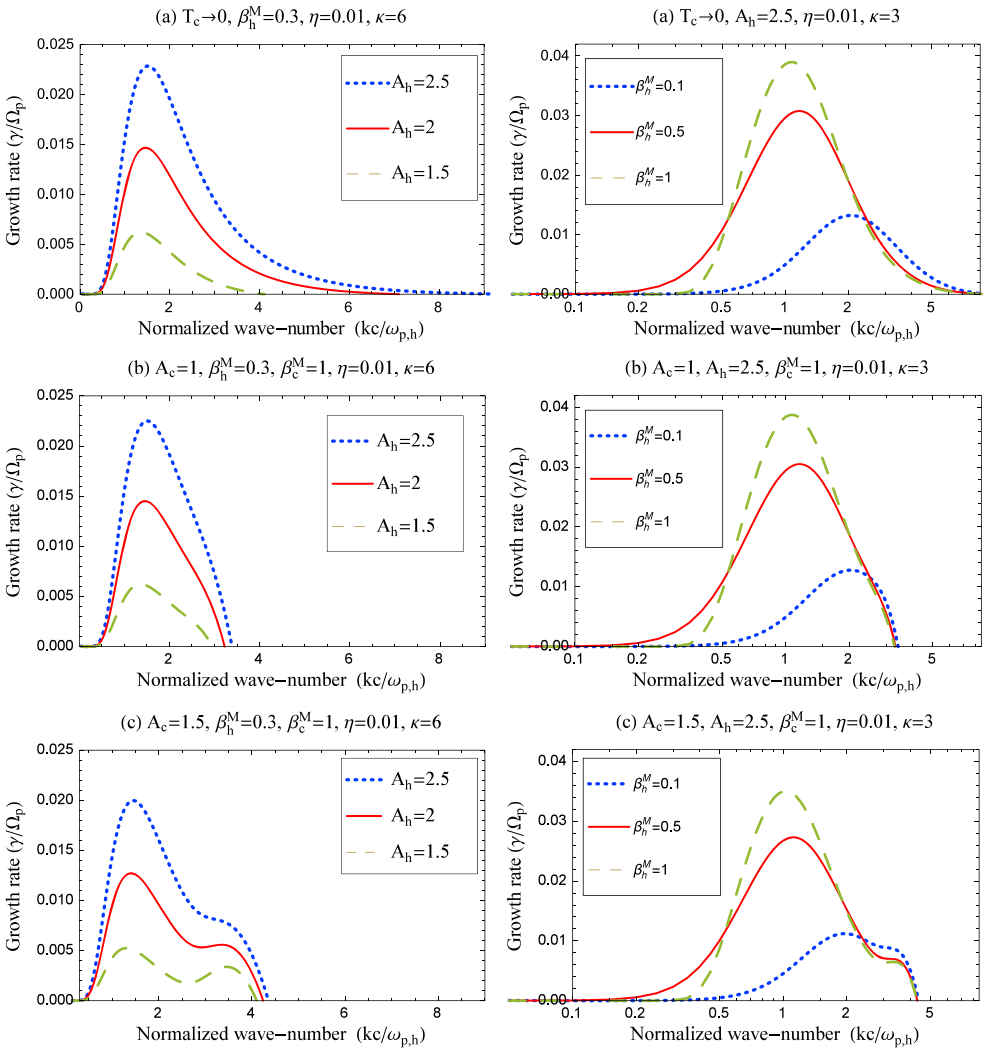

Figure 3. Effects of (left column) the halo anisotropy $A_h = 1.5, 2, 2.5$ and (right column) the halo plasma beta $\beta_h^M = 0.1, 0.5, 1$ on the growth rates of the EMIC instability. The plasma parameters and models considered for the core are explicitly given in each panel.

unstable wave numbers. The main distinct conditions analyzed here are determined by the plasma parameters which characterize these two populations in the solar wind. The existing observational data provide representative (mean or limit) values making a distinct characterization of the core and halo populations only for the solar wind electrons, while the proton data are limited to the core component. To characterize the proton halo, we invoke values deduced indirectly from the electrons and other complementary data. Thus, two representative values of the halo-core density ratio, $\eta = 0.01$ and 0.05 found relevant for the solar wind electrons, are also adopted here for protons on the basis of charge neutrality condition. For the proton core, values of the temperature anisotropy A_c and parallel plasma beta $\beta_{c,\|}$ are extracted from the histograms built by *Kasper et al.* [2003] with 1.6 million observations in slow winds ($V_{SW} < 400$ km/s) collected by Wind during a long interval of time between 1994 and 2001. The proton core concentrates to states of energy equipartition $\beta_c \simeq 1$ with a moderate temperature anisotropy (driving EMIC modes), usually satisfying $A_c < 2$. Spectral characteristic of the suprathermal populations are, in general, similar for both electrons and protons [*Christon et al.*, 1989], although for ions, the most probably values of the power index κ are, in general, higher than those found for electrons [*Collier et al.*, 1996]. More tenous than the core, the suprathermal halo may also be more anisotropic and expected to concentrate at lower values of the plasma beta parameter $\beta_{h,\|} < \beta_{c,\|}$.

Figures 1 and 2 present the unstable EMIC solutions, the growth rates, and wave frequencies, respectively, providing a suggestive comparison between the realistic approach proposed in the present paper and

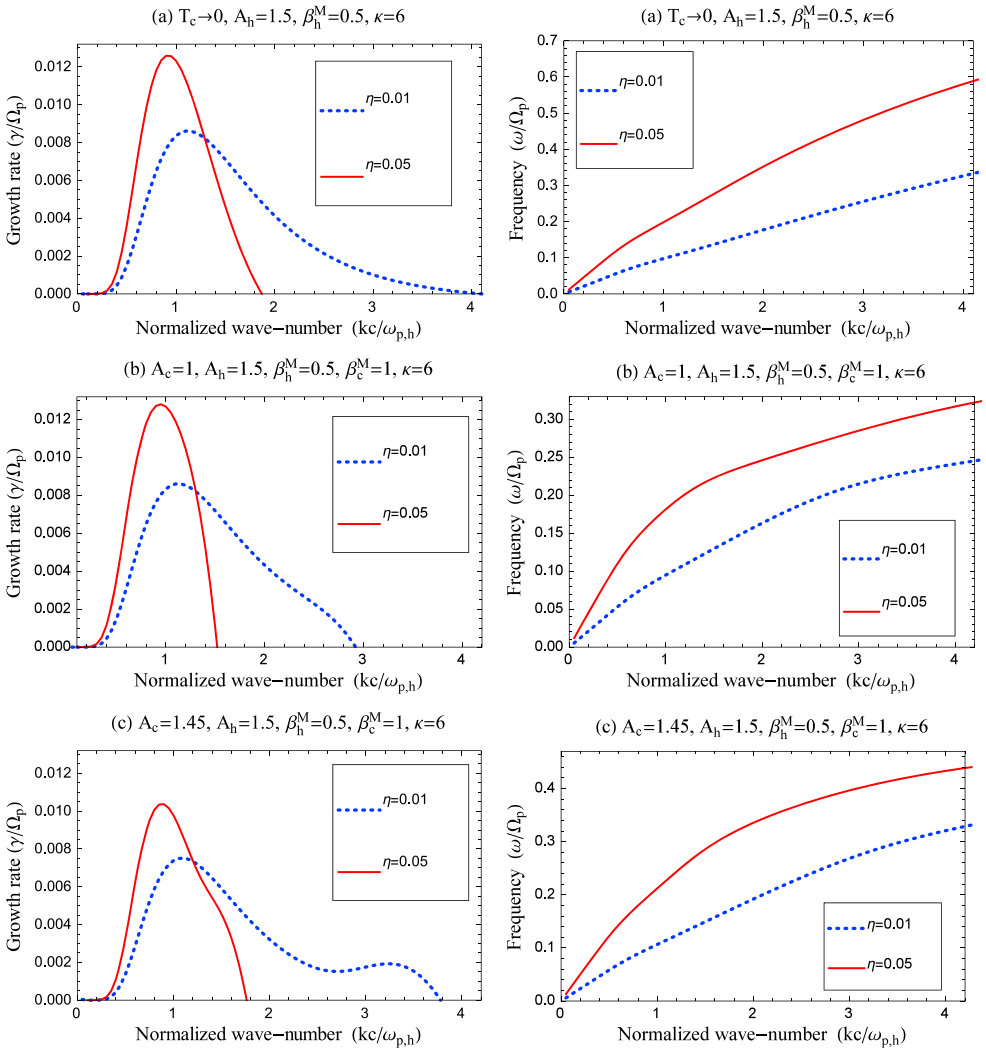

Figure 4. Effects of the halo-core density ratio $\eta = 0.05$ and 0.01 on the growth rates and wave frequencies of the EMIC instability. The plasma parameters and models considered for the core are explicitly given in each panel.

the simplified approaches considered before, e.g., a cold core plus a bi-Kappa halo [*Xiao et al.*, 2007] and two-Maxwellian models [*Gary et al.*, 1996]. If the core is considered cold ($T_c \to 0$, an assumption completely unrealistic for the solar wind), all the EMIC mode features, namely, growth rates, wave frequencies, and wave numbers are significantly overestimated. Otherwise, the instability driven by the halo anisotropy ($A_h > 1$) is inhibited by a finite thermal spread in the core, see the case with isotropic core. An additional anisotropy of the core $A_c > 1$ may considerably enhance the instability, increasing the growth rates, the range of unstable wave numbers, and the wave frequencies. When both the halo and core components are anisotropic, two peaks of the growth rates may become visible, the first at lower wave numbers is driven by the anisotropic halo, while the second peak is driven by the anisotropic core. The second peak becomes apparent and may exceed the halo peak only when the influence (or the presence) of the suprathermals, quantified in this case by two parameters η and κ, is diminished, i.e., for lower values of the halo-core relative density, e.g., $\eta = 0.01$, and high values of the power index, e.g., $\kappa = 6, \infty$. As expected, the difference between these peaks becomes less important in the limit of a Maxwellian halo ($\kappa \to \infty$). If we increase the presence of suprathermals by increasing the halo-core relative density to $\eta = 0.05$, the growth rates restrain to low wave numbers and exhibit only one peak driven by the suprathermal halo. The EMIC wave frequency is not much sensitive to the power index κ, but the growth rates are, in general, stimulated and the unstable wave numbers extend to markedly lower values with a decrease of this parameter.

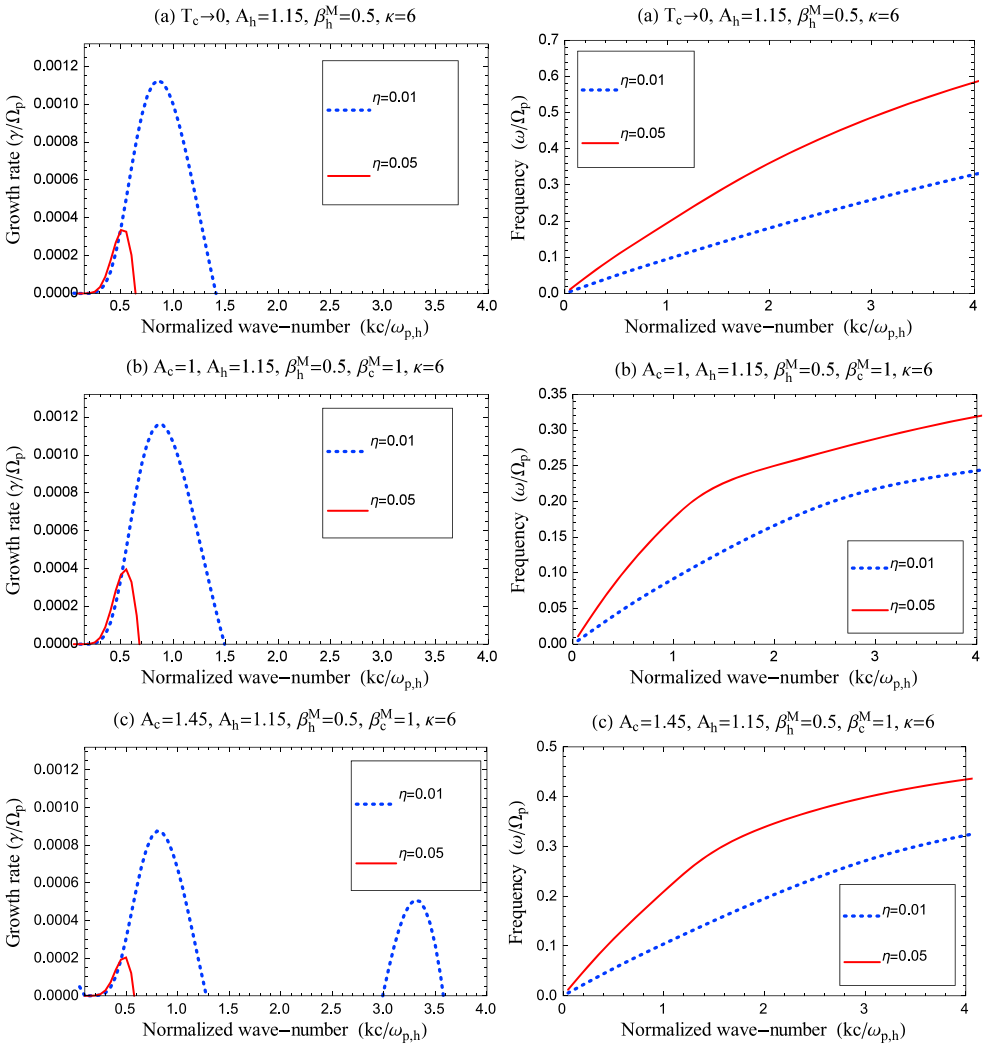

Figure 5. The same as in Figure 4 but for a lower anisotropy of the halo component $A_h = 1.15$.

We can already notice that suprathermals may have an important destabilizing effect on the EMIC modes, and in many situations this effect appears to be more significant than that produced by the core. Therefore, in the next three figures, Figures 3–5, we describe in detail the influence of the halo parameters, i.e., A_h, $\beta_{h,\|}$, and η, on the EMIC instability. This influence may, however, be highly dependent on the core properties, as shown already in Figures 1 and 2, and for that reason we keep in the next comparative analysis all the three models for the core, i.e., cold, isotropic, and anisotropic. Figure 3 shows a monotonic increase of the (maximum) growth rates with the increase of anisotropy $A_h = 1.5, 2, 2.5$ or the increase of parallel plasma beta $\beta_h^M = 0.1, 0.5, 1$. The second peak stimulated by the anisotropic core, see Figure 3c, remains dominated by the first peak driven by the more anisotropic halo.

The results presented in Figures 1 and 2 suggest that the halo-core density ratio η may play as a key factor in stimulating or suppressing the growth rates. In Figures 4 and 5 we examine the effect of the halo-core density ratio by taking two representative values $\eta = 0.05$ and 0.01. The EMIC solutions displayed in Figure 4, including both the growth rate and the wave frequency, are derived for maximum growth rates in the vicinity of $\gamma_m = 10^{-2}\Omega_p$. The same three models are considered for the core, and the unstable solutions are obtained for $\beta_h^M = 0.5$, $A_h = 1.5$, $\beta_c^M = 1$, and $\kappa = 6$. In all these cases the growth rates and the wave frequencies are enhanced by increasing the relative density of halo population from $\eta = 0.01$ to 0.05. However, the range of unstable wave numbers is considerably reduced by the same increase of η. The growth rate shows a second peak when the core anisotropy is large enough and comparable to the halo anisotropy, i.e., $A_c = 1.45$. In Figure 5 we extend this examination for the same plasma parameters as in Figure 4, but for a lower anisotropy

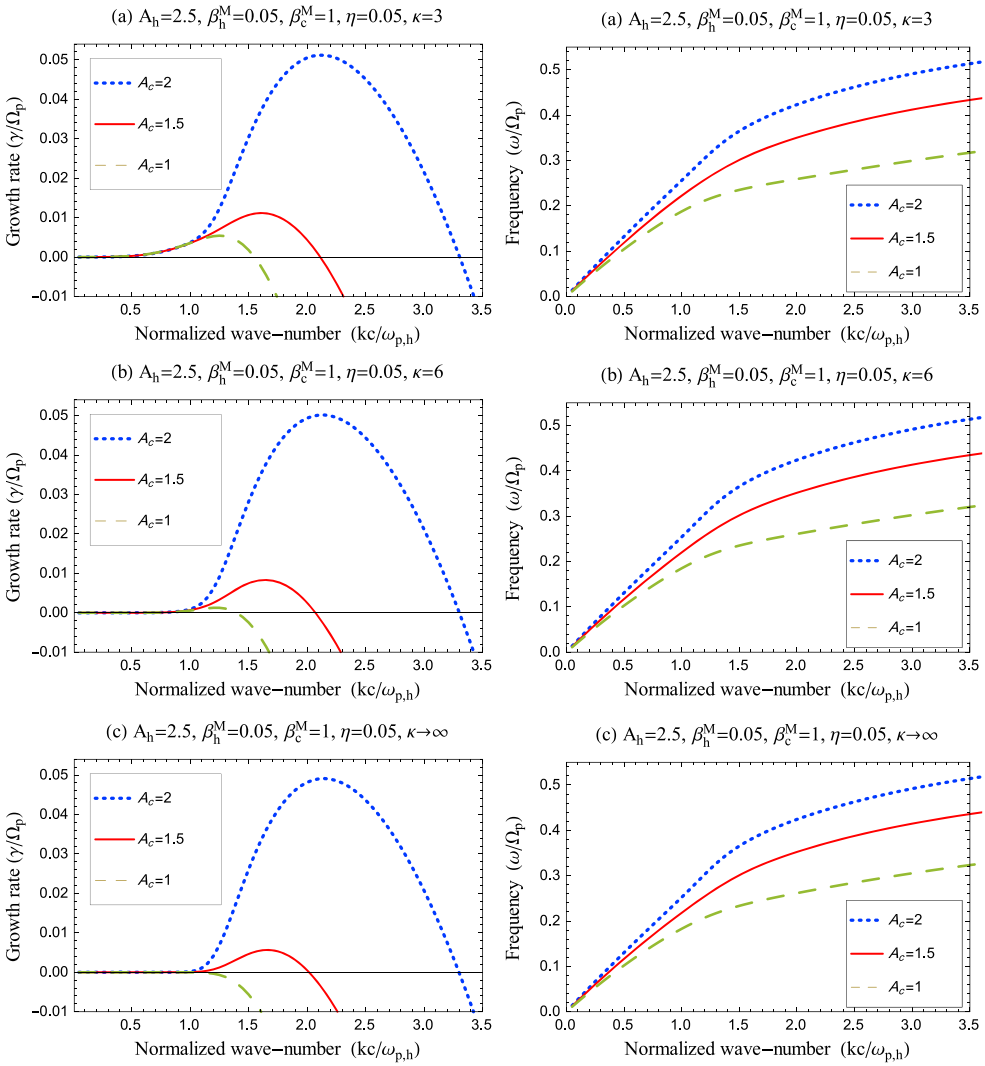

Figure 6. Effects of the anisotropic core $A_c = 2, 1.5, 1$ on the growth rate and the wave frequency of the EMIC instability. The plasma parameters and models considered for the core and halo components are explicitly given in each panel.

$A_h = 1.15$ yielding unstable solutions with lower values of the maximum growth rate in the vicinity of $\gamma_m = 10^{-3}\Omega_p$. In this case the increase of relative density η has an opposite influence, lowering the growth rates and the range of unstable wave numbers and wave frequencies. If it appears, the core peak is again dominated by the halo peak, although the core anisotropy $A_c = 1.45$ is (maybe unrealistically) higher than the halo anisotropy.

In Figure 6 we show the effect of the core anisotropy $A_c = 1, 1.5, 2$ on the EMIC instability mainly driven the anisotropic halo anisotropy with $A_h = 2.5$, $\beta_h^M = 0.05$, $\eta = 0.05$, and different power index $\kappa = 3, 6, \infty$. Both the growth rate and the wave frequency are enhanced by increasing the core anisotropy, and this effect is stimulated by the suprathermals, by decreasing the power index κ. The EMIC modes are stable (damped modes) for a two-Maxwellian model ($\kappa \to \infty$) with an isotropic core ($A_c = 1$), a case studied by *Gary et al.* [1994], but the instability develops for lower values of $\kappa = 6, 3$. Moreover, the relative halo population is high enough $\eta = 0.05$, preventing the growth rates to develop a second peak.

Now we have to remember that our present analysis assumes a Kappa distributed halo with κ-dependent temperature, see section 2. There is also an alternative method widely used in the investigations of suprathermal populations modeled with the same Kappa distribution functions but with κ-independent temperature. However, according to recent studies [*Lazar et al.*, 2015b, 2016], a Kappa distributed halo with κ-dependent temperature enables a more realistic interpretation of the suprathermal populations and their effects, e.g., on

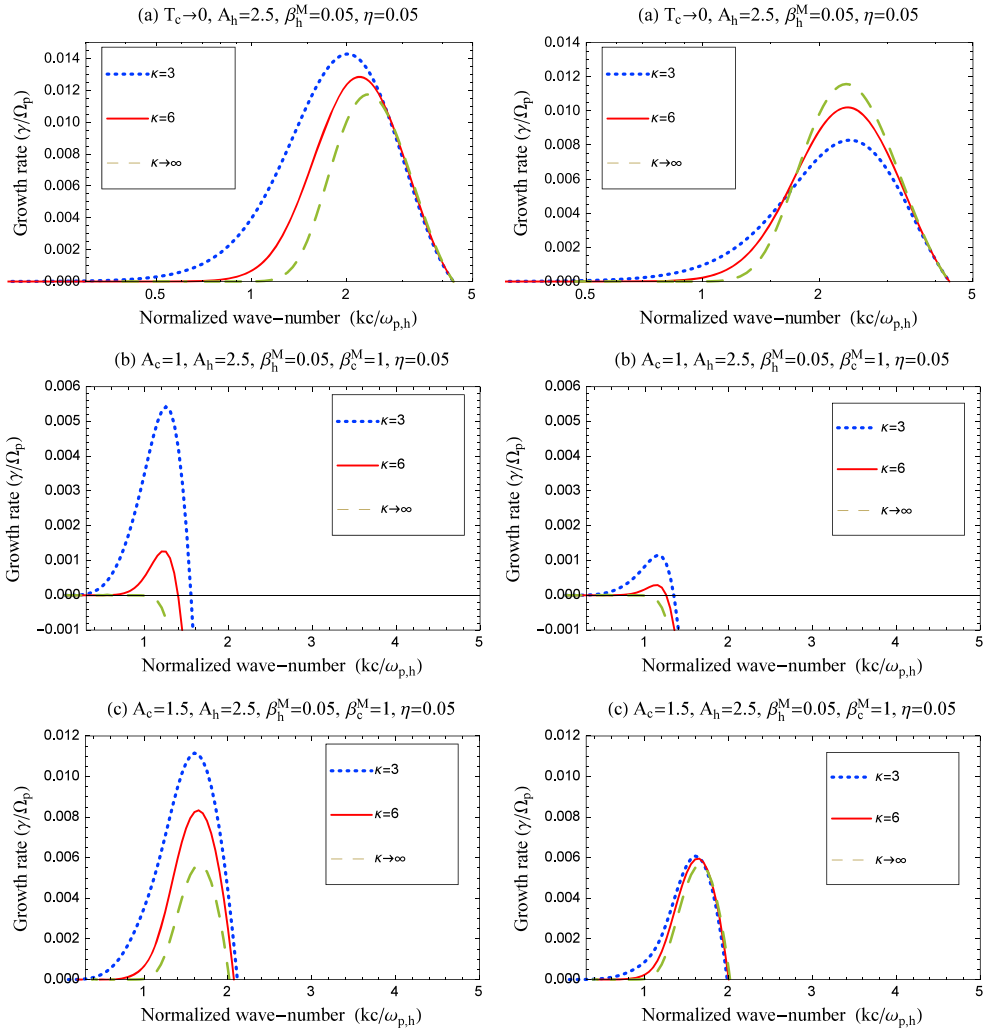

Figure 7. Growth rates of the EMIC instability: a comparison between the two Kappa approaches with (left column) κ-dependent temperature and (right column) κ-independent temperature. The plasma parameters and models considered for the core are explicitly given in each panel.

the kinetic instabilities. Figure 7 provides a comparative characterization of the EMIC solutions obtained with these two Kappa approaches. Figures 7 (left column) display the EMIC growth rates obtained for the Kappa model used in this work, i.e., with $T^K_{h,\|,\perp} > T^M_{h,\|,\perp}$. These growth rates show a systematic enhancement with the decrease of κ index, which seems to confirm the expectation that kinetic instabilities may be stimulated by the excess of free energy of the suprathermals. In Figure 7 (right) we display the growth rates derived for the same plasma parameters but using a Kappa approach with $T^K_{h,\|,\perp} = T^M_{h,\|,\perp}$. In this case it becomes complicated to decode the effect of suprathermal populations quantified by the power index κ. *Lazar et al.* [2015b] have already noticed that contrary to the expectations, these cyclotron instabilities of the EMIC or EMEC modes are, in general, inhibited for lower values of κ. Only the very small growth rates close to the marginal stability ($\gamma \to 0$) are enhanced by the suprathermals. Such a nonuniform influence of the suprathermals can be recognized in Figure 7. Thus, the growth rates obtained for a cold core (Figure 7a) are stimulated at low wave numbers, but their peaks obtained at higher wave numbers are considerably inhibited by lowering the power index κ. For a core with a finite thermal spread, the influence of suprathermals is opposite, especially that shown by the peaks obtained for an isotropic core (Figure 7b), while for an anisotropic core this influence seems to be again the function of the wave number value (Figure 7c).

3.2. The Instability Thresholds

In Figures 8 and 9 we display the instability thresholds as isocontours of the maximum growth rates at two distinct levels, $\gamma_m/\Omega_p = 10^{-3}$ and 10^{-2}, the lower one approaching the marginal stability of the EMIC modes.

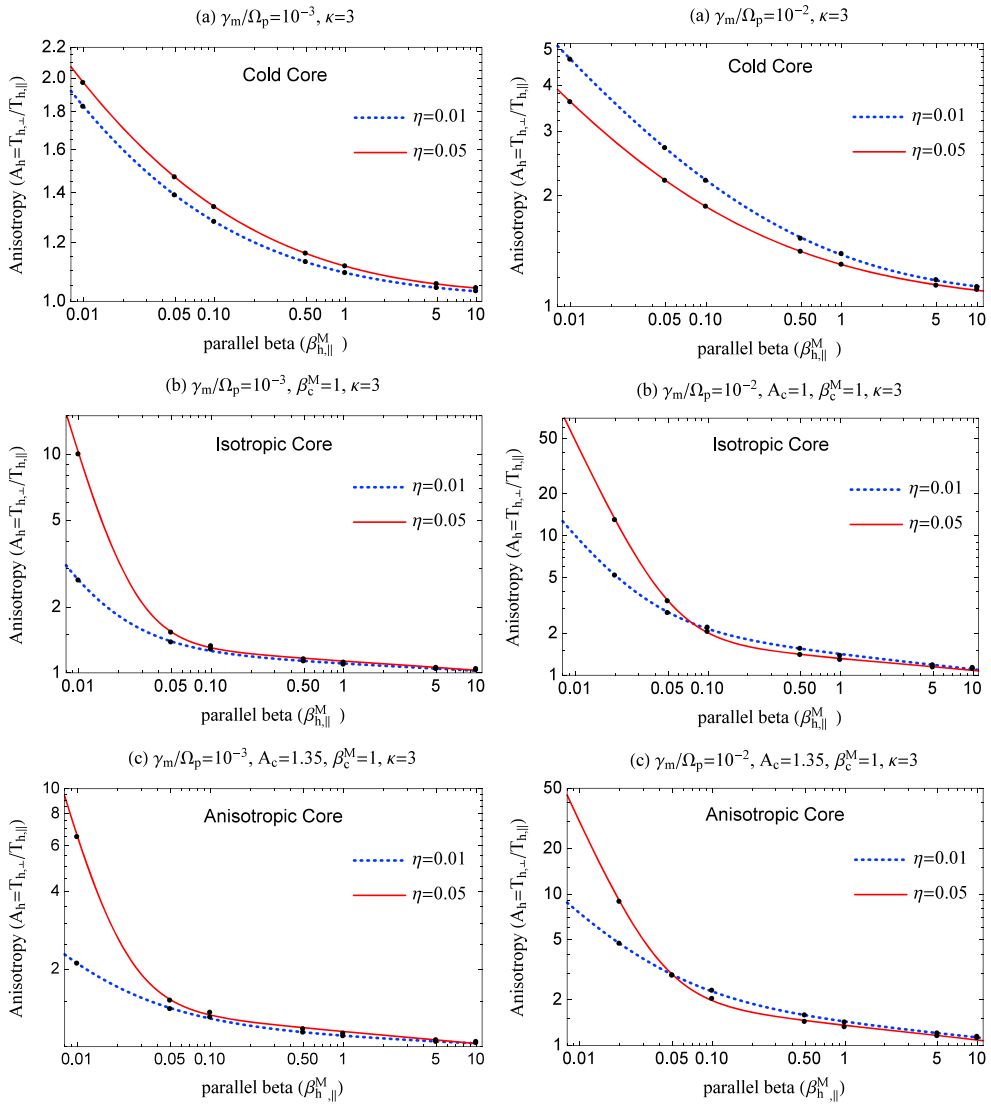

Figure 8. Effects of the halo-core density ratio $\eta = 0.05, 0.01$ on the EMIC thresholds (left) $\gamma = 10^{-3}\Omega_p$ and (right) $\gamma = 10^{-2}\Omega_p$. The plasma parameters and models considered for the core are explicitly given in each panel.

These thresholds provide a more comprehensive picture for the properties of the EMIC instability under the interplay of the core and suprathermal populations, for extended conditions satisfied by the suprathermal halo populations in the solar wind and planetary magnetospheres, e.g., $0.01 < \beta_{h,\|} < 10$. The comparative analysis include the effects of the halo-core density ratio η in Figure 8 and the power index κ in Figure 9 and make a clear distinction between the same three models considered above for the core, namely, cold core ($T_c \to 0$), isotropic $A_c = 1$, or anisotropic with $A_c > 1$. The EMIC thresholds are obtained with an inverse correlation law between the temperature anisotropy A_h and the parallel plasma beta $\beta^M_{h,\|}$

$$A_h = \left(1 + \frac{a}{\beta^{M\ b}_{h,\|}}\right)\frac{c}{\beta^{M\ d}_{h,\|}}, \tag{17}$$

where the values of the fitting parameters a, b, c, and d are provided in Tables 1–4. The classical case of the inverse correlation law introduced by *Gary and Lee* [1994] is recovered as for particular values of $c = 1$ and $d = 0$.

The effect of the halo-core density ratio η on the instability thresholds in Figure 8 is not uniform, being highly dependent of $\beta^M_{h,\|}$ and A_h. A more dense halo is expected to lower the instability thresholds, and this is effect is

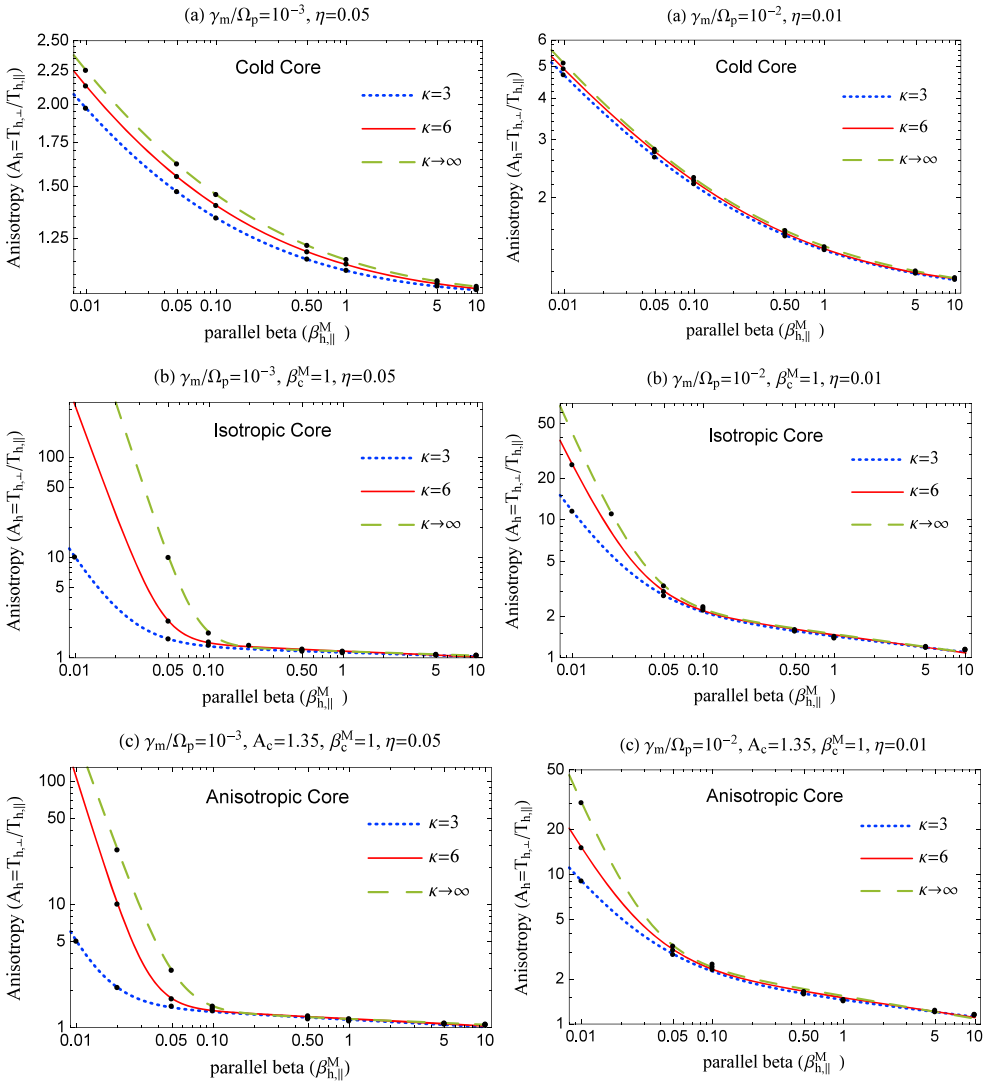

Figure 9. Effects of the power index $\kappa = 3, 6, \infty$ on the EMIC thresholds (left) $\gamma = 10^{-3}\Omega_p$ with $\eta = 0.05$ and (right) $\gamma = 10^{-2}\Omega_p$ with $\eta = 0.01$. The plasma parameters and models considered for the core are explicitly given in each panel.

indeed confirmed for sufficiently large values of $\beta^M_{h,\parallel} > 0.1$. For lower values of $\beta^M_{h,\parallel} < 0.1$ the kinetic effects are dominated by the core, and the instability thresholds conditioned by the halo component increase considerably. The instability thresholds are also lowered by the suprathermal populations quantified by the power index κ in Figure 9. This effect is again more significant for lower values of $\beta^M_{h,\parallel} < 0.1$, when the main free energy of the halo component resides in the suprathermal tails and not in the thermal spread of this component. Naturally, the influence of suprathermals diminishes with decreasing the relative halo-core density

Table 1. Fitting Parameters for Thresholds $\gamma_m/\Omega_p = 10^{-3}$ in Figure 8

Core Model	η	a	b	c	d
Cold	0.01	0.094	0.472	1	0
	0.05	0.118	0.456	1	0
Isotropic	0.01	0.0121	1.223	1.402	0.104
	0.05	0.0028	1.957	1.315	0.084
Anisotropic	0.01	0.0461	0.876	1.372	0.087
	0.05	0.0021	1.894	1.353	0.096

Table 2. Fitting Parameters for Thresholds $\gamma_m/\Omega_p = 10^{-2}$ in Figure 8

Core Model	η	a	b	c	d
Cold	0.01	0.390	0.488	1	0
	0.05	0.292	0.473	1	0
Isotropic	0.01	0.388	0.480	0.0002	2.052
	0.05	0.287	0.417	0.0065	1.789
Anisotropic	0.01	0.419	0.478	0.0005	1.632
	0.05	0.318	0.450	0.0016	1.944

(Figure 9, right column). The instability thresholds confirm the effects of η and κ parameters on the growth rates found in the particular cases from section 3.1. In the cold core limit the growth rates are overestimated but the instability thresholds are, implicitly, underestimated.

4. Concluding Discussions

We have refined the linear kinetic approach of the EMIC instability on the basis of an advanced modeling of the proton velocity distribution in accord with the observations in the solar wind. The low-frequency fluctuations detected in the solar wind may be enhanced locally by this instability driven by the anisotropic protons. Moreover, in the absence of energetic events the in situ measurements reveal a dual structure of the velocity distributions of plasma particles, with a thermal (Maxwellian) core and a suprathermal (Kappa) halo. Each of these two components can exhibit temperature anisotropy and implicitly drive instabilities of the EMIC modes. Many studies of this instability that claim applicability in the solar wind, are in general based on simplified models of the velocity distributions, minimizing or just ignoring effects of suprathermal populations. In the present paper we have shown that a realistic approach of this instability in the solar wind conditions must take into account the suprathermal protons, which may significantly change the instability conditions.

The EMIC unstable solutions analyzed in section 3 are derived for plasma parameters typically encountered in the solar wind. These solutions are provided not only for the realistic approach proposed in the present paper but for a number of simplified models considered before, e.g., a cold core plus a bi-Kappa (or bi-Maxwellian) halo or two-Maxwellian models, enabling us to make a comparative analysis and outline the interplay of the core and halo populations and their influence on the growth rates, wave frequency, and the unstable wave numbers. Thus, the main properties of the EMIC instability, namely, growth rates, wave frequencies, and wave numbers are markedly overestimated when the core is considered cold ($T_c \to 0$), an assumption completely unrealistic for the solar wind. Otherwise, the instability driven by the halo anisotropy $A_h > 1$ is inhibited by a finite thermal spread in the core but can be stimulated by the anisotropy of the proton core $A_c > 1$. The growth rates may therefore show a second distinct peak of the unstable EMIC modes driven by the anisotropic core at larger wave numbers. The occurrence of the core peak is directly conditioned by an increase of the core population (i.e., relative to the halo by decreasing η) and an enhancement of the core anisotropy. Growth rates with two peaks are also obtained for a two-Maxwellian approach, i.e., Maxwellian core plus Maxwellian halo ($\kappa \to \infty$), but here we have shown that the halo peak is significantly enhanced by the suprathermal

Table 3. Fitting Parameters for Thresholds $\gamma_m/\Omega_p = 10^{-3}$ with $\eta = 0.05$ in Figure 9

Core Model	κ	a	b	c	d
Cold	3	0.118	0.456	1	0
	6	0.140	0.452	1	0
	∞	0.162	0.443	1	0
Isotropic	3	0.00031	2.148	1.131	0.041
	6	0.00001	3.543	1.162	0.054
	∞	0.00003	4.044	1.160	0.043
Anisotropic	3	0.00004	2.373	1.159	0.0595
	6	5×10^{-6}	3.532	1.176	0.058
	∞	0.00012	3.040	1.175	0.047

Table 4. Fitting Parameters for Thresholds $\gamma_m/\Omega_p = 10^{-2}$ with $\eta = 0.01$ in Figure 9

Core Model	κ	a	b	c	d
Cold	3	0.380	0.493	1	0.0
	6	0.399	0.494	1	0.0
	∞	0.409	0.499	1	0.0
Isotropic	3	0.0069	1.370	1.419	1.370
	6	0.0014	1.887	1.461	0.130
	∞	0.0010	2.076	1.481	0.132
Anisotropic	3	0.0188	1.091	1.424	0.106
	6	0.0052	1.469	1.489	0.129
	∞	0.0011	1.945	1.536	0.150

populations quantified by the low values of κ index. In addition, the effect of the halo-core relative density η on the growth rate, real frequency, and the instability thresholds is found to be dependent on the halo temperature anisotropy and the plasma beta parameter of this component. A series of punctual conclusions that are evident from Figures 1 to 9 may be itemized as follows: (a) Growth rates increase with decreasing κ (i.e., broader suprathermal distribution). (b) Growth rates increase with increasing suprathermal anisotropy. (c) Growth rates increase with increasing core anisotropy. (d) Growth rates increase with increasing suprathermal beta. (e) When suprathermal anisotropy is high, growth rates increase with increasing suprathermal/core relative abundance. (f) When suprathermal anisotropy is low, growth rates decrease with increasing suprathermal/core relative abundance. (g) A higher suprathermal fraction requires a higher suprathermal anisotropy to reach an instability threshold. and (h) A lower κ requires a lower (halo) anisotropy to reach an instability threshold.

It becomes clear that the presence of suprathermal populations in conditions specific to the solar wind and planetary magnetosphere has an important impact on the EMIC instability. We have found an significant contrast between the instability conditions resulted from the interplay of the core and halo populations and those predicted by simplified models which neglect either the presence of suprathermal populations or the thermal spread of the core. By this, the results of the present paper demonstrate that the existing interpretations of this instability, especially the instability conditions and the role played by the EMIC modes in key processes in space plasmas, must be reconsidered. An important aspect that we plan to re-evaluate in the future studies is the energy transfer mediated by these instabilities between suprathermal and thermal components. Moreover, the next immediate extension of the present study should include the effects of alpha particles, which may have a interesting influence on the EMIC instability conditions in the solar wind. The heating and acceleration scenarios with alpha particles and heavier ions playing an essential role focus on the energy supply by the EMIC waves to heat the solar wind ions and produce the fast winds in coronal conditions. The expectations are also that our present results will stimulate new investigations to unveil the quasilinear and nonlinear regimes of this instability, enabling not only a comprehensive description but also, mainly, a realistic prediction of its potential implication in key processes in the solar wind. Besides the linear kinetic approach reported here, the nonlinear studies of these modes are needed mainly because of their capability to describe the nonlinear saturation state of the instability and the effects of wave-particle interaction on the distributions and to estimate the amount of heating and acceleration of the plasma ions [*Ofman and Viñas*, 2007].

Acknowledgments
The authors acknowledge support from the Katholieke Universiteit Leuven, the Ruhr-University Bochum, and Alexander von Humboldt Foundation. These results were obtained in the framework of the projects GOA/2015-014 (KU Leuven), G0A2316N (FWO-Vlaanderen), and C 90347 (ESA Prodex 9). The research leading to these results has also received funding from IAP P7/08CHARM (Belspo) and the European Commission's Seventh Framework ProgrammeFP7-PEOPLE-2010-IRSES-269299 project-SOLSPANET (www.solspanet.eu). S.M. Shaaban would like to thank the Egyptian Ministry of Higher Education for supporting his research activities. This paper is theoretical and does not contain observational or simulation data.

References

Araneda, J. A., E. Marsch, and F. Adolfo (2008), Proton core heating and beam formation via parametrically unstable Alfvé-cyclotron waves, *Phys. Rev. Lett.*, *100*, 125003.

Astfalk, P., T. Görler, and F. Jenko (2015), DSHARK: A dispersion relation solver for obliquely propagating waves in bi-kappa-distributed plasmas, *J. Geophys. Res. Space Physics*, *120*, 7107–7120, doi:10.1002/2015JA021507.

Bruno, R., and V. Carbone (2013), The solar wind as a turbulence laboratory, *Living Rev. Sol. Phys.*, *10*, 2.

Christon, S. P., D. J. Williams, D. G. Mitchell, L. A. Frank, and C. Y. Huang (1989), Spectral characteristics of plasma sheet ion and electron populations during undisturbed geomagnetic conditions, *J. Geophys. Res.*, *94*, 13,409–13,424.

Christon, S. P., D. J. Williams, D. G. Mitchell, C. Y. Huang, and L. A. Frank (1991), Spectral characteristics of plasma sheet ion and electron populations during disturbed geomagnetic conditions, *J. Geophys. Res.*, *96*, 1–22.

Collier, M. R., D. C. Hamilton, G. Gloeckler, P. Bochsler, and R. B. Sheldon (1996), Neon-20, oxygen-16, and helium-4 densities, temperatures, and suprathermal tails in the solar wind determined with WIND/MASS, *Geophys. Res. Lett.*, *23*, 1191–1194.

Cornwall, J. M., and M. Schulz (1971), Electromagnetic ion-cyclotron instabilities in multicomponent magnetospheric plasmas, *J. Geophys. Res.*, *76*, 7791–7796.
dos Santos, M. S., L. F. Ziebell, and R. Gaelzer (2015), Ion-cyclotron instability in plasmas described by product-bi-kappa distributions, *Phys. Plasma*, *22*, 122107.
Feldman, W. C., J. R. Asbridge, S. J. Bame, and M. D. Montgomery (1973), Double ion streams in the solar wind, *J. Geophys. Res.*, *78*, 2017–2027.
Feldman, W. C., J. R. Asbridge, S. J. Bame, M. D. Montgomery, and S. P. Gary (1975), Solar wind electrons, *J. Geophys. Res.*, *80*, 4181–4196.
Fried, B. D., and S. D. Conte (1961), *The Plasma Dispersion Function*, Academic Press, New York.
Gary, S. P. (1993), *Theory of Space Plasma Microinstabilities*, Cambridge Univ. Press, Cambridge, U. K.
Gary, S. P., and M. A. Lee (1994), The ion cyclotron anisotropy instability and the inverse correlation between proton anisotropy and proton beta, *J. Geophys. Res.*, *99*, 11,297–11,301.
Gary, S. P., M. B. Moldwin, M. F. Thomsen, D. McComas, and Winske D. J. (1994), Hot proton anisotropies and cool proton temperatures in the outer magnetosphere, *J. Geophys. Res.*, *99*, 23,603–23,615.
Gary, S. P., V. M. Vazquez, and D. Winske (1996), Electromagnetic proton cyclotron instability: Proton velocity distributions, *J. Geophys. Res.*, *101*, 13,327–13,333.
Hellberg, M., R. Mace, and T. Cattaert (2005), Effects of superthermal particles on waves in magnetized space plasmas, *Space Sci. Rev.*, *121*, 127–139.
Hellinger, P., and P. Trávníček (2005), Magnetosheath compression: Role of characteristic compression time, alpha particle abundance, and alpha/proton relative velocity, *J. Geophys. Res.*, *110*, A04210, doi:10.1029/2004JA010687.
Hellinger, P., and P. Trávníček (2011), Proton core-beam system in the expanding solar wind: Hybrid simulations, *J. Geophys. Res.*, *116*, A11101, doi:10.1029/2011JA016940.
Jian, L. K., C. T. Russell, J. G. Luhmann, R. J. Strangeway, J. S. Leisner, and A. B. Galvin (2009), Ion cyclotron waves in the solar wind observed by stereo near 1 AU, *Astrophys. J. Lett.*, *701*, L105.
Kennel, C. F., and H. E. Petschek (1966), Limit on stably trapped particle fluxes, *J. Geophys. Res.*, *71*, 1–28.
Kasper, J. C., A. J. Lazarus, S. P. Gary, and A. Szabo (2003), Solar wind temperature anisotropies, *AIP Conf. Proc. 679*, 538–541.
Lazar, M., R. Schlickeiser, and P. K. Shukla (2008), Cumulative effect of the Weibel-type instabilities in symmetric counterstreaming plasmas with kappa anisotropies, *Phys. Plasmas*, *15*, 042103.
Lazar, M. (2012), The electromagnetic ion-cyclotron instability in bi-Kappa distributed plasmas, *Astron. Astrophys.*, *547*, A94.
Lazar, M., and S. Poedts (2014), Instability of the parallel electromagnetic modes in Kappa distributed plasmas—II. Electromagnetic ion–cyclotron modes, *MNRAS*, *437*, 641–648.
Lazar, M., R. Schlickeiser, and S. Poedts (2012), Suprathermal Particle Populations in the Solar Wind and Corona, in *Exploring the Solar Wind*, edited by M. Lazar, p. 241, InTech, Rijeka, Croatia. [Available at http://www.intechopen.com/books/exploring-the-solar-wind/.]
Lazar, M., S. Poedts, and R. Schlickeiser (2014), The interplay of Kappa and core populations in the solar wind: Electromagnetic electron cyclotron instability, *J. Geophys. Res. Space Physics*, *119*, 9395–9406, doi:10.1002/2014JA020668.
Lazar, M., S. Poedts, R. Schlickeiser, and C. Dumitrache (2015a), Towards realistic parametrization of the kinetic anisotropy and the resulting instabilities in space plasmas: Electromagnetic electron-cyclotron instability in the solar wind, *MNRAS*, *446*, 3022–3033.
Lazar, M., S. Poedts, and H. Fichtner (2015b), Destabilizing effects of the suprathermal populations in the solar wind, *Astron. Astrophys.*, *582*, A124.
Lazar, M., H. Fichtner, and P. H. Yoon (2016), On the interpretation and applicability of κ-distributions, *Astron. Astrophys.*, *589*, A39.
Lin, R. P. (1998), Wind observations of suprathermal electrons in the interplanetary medium, *Space Sci. Rev.*, *86*, 61–78.
Maksimovic, M., V. Pierrard, and P. Riley (1997), Ulysses electron distributions fitted with Kappa functions, *Geophys. Res. Lett.*, *24*, 1151–1154.
Maksimovic, M., S. P. Gary, and R. M. Skoug (2000), Solar wind electron suprathermal strength and temperature gradients: Ulysses observations, *J. Geophys. Res.*, *105*, 18,337–18,350.
Maksimovic, M., et al. (2005), Radial evolution of the electron distribution functions in the fast solar wind between 0.3 and 1.5 AU, *J. Geophys. Res.*, *110*, A09104, doi:10.1029/2005JA011119.
Maneva, Y. G., L. Ofman, and A. Viñas (2015), Relative drifts and temperature anisotropies of protons and α particles in the expanding solar wind: 2.5 D hybrid simulations, *Astron. Astrophys.*, *578*, A85.
Mangeney, A., C. Salem, P. Veltri, and C. Cecconi (2001), Intermittency in the solar wind turbulence and the Haar wavelet transform, in *Sheffield Space Plasma Meeting: Multipoint Measurements Versus Theory*, edited by B. Warmbein, *Eur. Space Agency Spec. Publ., 492*, 53 pp., Noordwijk, Netherlands.
Marsch, E. (2006), Kinetic physics of the solar corona and solar wind, *Living Rev. Sol. Phys.*, *3*, 1. [Available at http://www.livingreviews.org/lrsp-2006-1.]
Marsch, E., K-H. Mühlhäuser, R. Schwenn, H. Rosenbauer, W. Pilipp, and F. M. Neubauer (1982), Solar wind protons: Three-dimensional velocity distributions and derived plasma parameters measured between 0.3 and 1 AU, *J. Geophys. Res.*, *87*, 52–72.
Matteini, L., S. Landi, P. Hellinger, F. Pantellini, M. Maksimovic, M. Velli, B. E. Goldstein, and E. Marsch (2007), Evolution of the solar wind proton temperature anisotropy from 0.3 to 2.5 AU, *Geophys. Res. Lett.*, *34*, L20105, doi:10.1029/2007GL030920.
Maruca, B. A., J. C. Kasper, and S. P. Gary (2012), Instability-driven limits on helium temperature anisotropy in the solar wind: Observations and linear Vlasov analysis, *Astrophys. J.*, *748*, 137.
Nieves-Chinchilla, T., and A. F. Viñas (2008), Solar wind electron distribution functions inside magnetic clouds, *J. Geophys. Res.*, *113*, A02105, doi:10.1029/2007JA012703.
Ofman, L., S. P. Gary, and A. Vinas (2002), Resonant heating and acceleration of ions in coronal holes driven by cyclotron resonant spectra, *J. Geophys. Res.*, *107*(A12), 1461, doi:10.1029/2002JA009432.
Ofman, L., and A. F. Viñas (2007), Two-dimensional hybrid model of wave and beam heating of multi-ion solar wind plasma, *J. Geophys. Res.*, *112*, A06104, doi:10.1029/2006JA012187.
Ofman, L., A. F. Viñas, and Y. Maneva (2014), Two-dimensional hybrid models of H^{+}-He^{++} expanding solar wind plasma heating, *J. Geophys. Res. Space Physics*, *119*, 4223–4238, doi:10.1002/2013JA019590.
Pierrard, V., M. Maksimovic, and J. Lemaire (1999), Electron velocity distribution functions from the solar wind to the corona, *J. Geophys. Res.*, *104*, 17,021–17,032.
Pierrard, V., and M. Lazar (2010), Kappa distributions: Theory and applications in space plasmas, *Sol. Phys.*, *267*, 153–174.
Shaaban, S. M., M. Lazar, S. Poedts, and A. Elhanbaly (2015), Effects of electrons on the electromagnetic ion cyclotron instability: Solar wind implications, *Astrophys. J.*, *814*, 34.
Shaaban, S. M., M. Lazar, S. Poedts, and A. Elhanbaly (2016), Effects of suprathermal electrons on the proton temperature anisotropy in space plasmas: Electromagnetic ion-cyclotron instability, *Astrophys. Space Sci.*, *361*, 1–12.

Sittler, E. C., Jr., and L. F. Burlaga (1998), Electron temperatures within magnetic clouds between 2 and 4 AU: Voyager 2 observations, *J. Geophys. Res.*, *103*, 17,447–17,454.

Summers, D., and R. M. Thorne (1991), The modified plasma dispersion function, *Phys. Plasmas*, *3*, 1835.

Vasyliunas, V. M. (1968), A survey of low-energy electrons in the evening sector of the magnetosphere with OGO 1 and OGO 3, *J. Geophys. Res.*, *73*, 2839–2884.

Xiao, F., Q. Zhou, H. He, H. Zheng, and S. Wang (2007), Electromagnetic ion cyclotron waves instability threshold condition of suprathermal protons by kappa distribution, *J. Geophys. Res.*, *112*, A07219, doi:10.1029/2006JA012050.